*32nd EPS Conference on Plasma Phys. Tarragona, 27 June - 1 July 2005 ECA Vol.**29C**, P-4.100 (2005)*

Transport studies in MAST with enhanced Doppler spectrometry

N. J. Conway, M. Wisse[1], R. J. Akers, C. Brickley,

P. G. Carolan, A. R. Field and M. J. Walsh

EURATOM/UKAEA Fusion Association, Culham Science Centre,
Abingdon, Oxon, OX14 3DB, UK
[1] *University College Cork, Cork, Ireland*

Introduction

Recently, there has been considerable progress with studies of the energy transport in high-β plasmas in both the MAST and NSTX Spherical Tokamak (ST) devices [1, 2], permitting quantitative comparisons with results from gyro-kinetic and MHD fluid simulations of the anomalous transport processes [3, 4]. After implementing some major improvements to diagnostic systems, MAST is now well equipped to advance these studies. Discharges produced in MAST with internal transport barriers (ITBs) have exhibited scale lengths in the temperature and density profiles which can approach the ion Larmor radius, ρ_i (~1 cm) [1, 5]. For example, in discharges with counter injected neutral beam heating (NBI), electron ITBs with T_e scale lengths, $L_T \sim \rho_i$ have been observed using the high-resolution 300 point Thomson Scattering (TS) system [6]. In this case it was not possible to determine whether the T_i profile exhibited similar scale lengths because of the limited spatial resolution (~ 4 cm) of the earlier Charge Exchange Recombination Spectroscopy (CXRS) diagnostic [7]. To meet this challenge, a new CXRS system utilising a high-throughput spectrometer with a total of 224 spatial channels has been implemented on MAST. This system is described below along with the results of some preliminary transport analyses which used data from this diagnostic.

The CXRS upgrade

The upgraded CXRS diagnostic on MAST is completely new, improvements having been made to all components of the system. One drawback of the previous system was that the collection optics, situated on the mid-plane, were in a position where many spatial channels viewed emission from both of the neutral beams but at different major radii from each. This was a particular problem in high-density H-mode plasmas, where the bright edge CXR emission from the secondary beam could dominate the weaker core emission from the primary beam for which the geometry was optimised. In order to circumvent this 'dazzle' effect, new ports were cut into the vessel above and below the mid-plane to provide tilted views (at ~15° to the horizontal) of each beam while passing above or below the other beam as shown in Fig 1.

For each view an f/2 collection lens couples light to 64×400 μm optical fibres, with one fibre per spatial channel. A third toroidal view looking away from the beams provides 32 additional channels to measure the 'passive' background emission. Two sets of in-vessel collection optics have also been implemented viewing each beam from above to provide poloidal measurements. Each of these has 64 spatial channels with 32 channels viewing the CXR emission from the beam and the other 32 the passive emission adjacent to the beam. The spatial resolution of both the toroidal and poloidal views is ~ 1 cm.

The Czerny-Turner spectrometer utilised by the old CXRS system had been selected for its ability to operate at wavelengths down to ~200 nm. However, this also dramatically reduced the available étendue of the system, as the collimating and focussing optics were simple spherical mirrors, with inherently poor off-axis aberrations. Since measurements are usually made using the CVI (529 nm, n = 7-8) emission line, which is located in a relatively

uncluttered region of the spectrum, a decision was made to optimise the new spectrometer for this wavelength. (The capability to operate across the visible spectrum from ~400 nm to ~700 nm is retained to permit occasional use with other emission lines and impurities.)

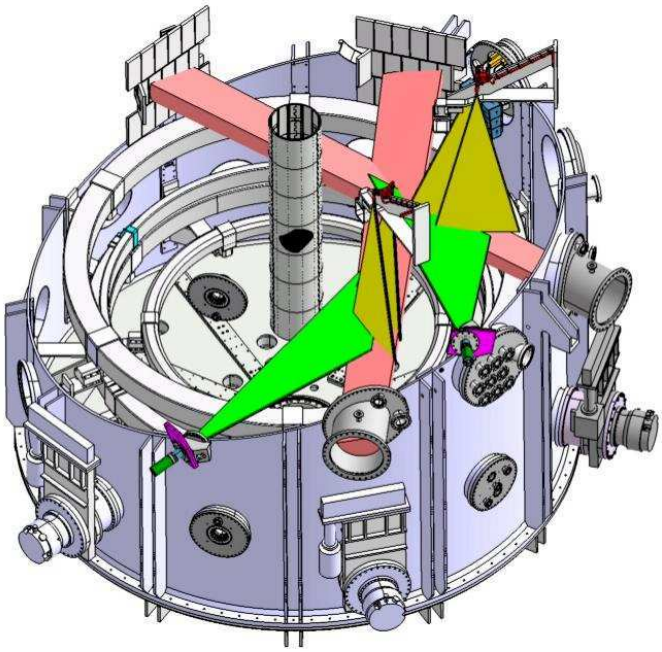

Figure 1: Schematic of the new off-midplane toroidal (green) and poloidal (yellow) CXRS views. The neutral beams are also shown (in pink).

The new spectrometer, which is shown in Fig. 2, utilises a large, custom-made holographic transmission grating [8] with very high diffraction efficiency (>80%). Transmission gratings also facilitate a highly compact design, permitting excellent off-axis optical coupling. High-quality SLR camera lenses are used for the collimating and focussing elements. The array of 224 fibres is arranged at the spectrometer input focal plane in a matrix with 7 vertical columns of 32 fibres. A narrow-band interference filter of ~ 3 nm bandwidth is used to prevent overlap of spectra from adjacent chords. This allows for measurement of ion temperatures up to ~ 5 keV and flow velocities up to ~ 500 km/s.

The spatial channels are distributed uniformly in major radius resulting in a radial resolution ΔR ~ 1 cm. Such high resolution is not required to resolve the profile gradients in the core region, where scale lengths are relatively large. Therefore, signal from several adjacent chords can be integrated here resulting in improved photon statistics. This helps to overcome the problem of the relatively weak CX emission from the core in discharges such as H-modes, as mentioned above.

The detector is a high-speed CCD camera system manufactured by Pixelvision, which utilises a back-illuminated sensor with 656×498 12 μm square pixels and excellent quantum efficiency of ~ 80% at 529 nm. It has four readout taps (one at each corner), each of which is digitised at 2.2 MHz, allowing real-time readout of the binned signal from all 224 spatial channels in <3.5 ms. Real-time readout overcomes the limitation on the number of frames

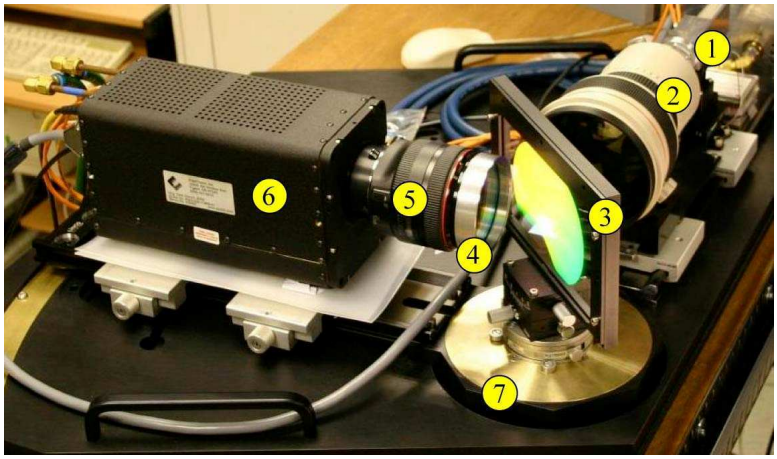

Figure 2: The new spectrometer: (1) Fibre array, 7 columns × 32 fibres/column, (2) Collimating lens (200mm, f/1.8), (3) 2600 l/mm transmission grating, (4) Narrowband interference filter, (5) Focussing lens (85mm, f/1.2), (6) Pixelvision CCD camera, (7) Movable camera arm & grating, allowing wavelength variation.

with the on-chip storage scheme used by the old system. In fact, the system is usually operated with a 5 ms integration period to match the 200Hz repetition rate of the 20-channel Nd-YAG TS system. The high étendue of the new spectrometer provides increased signal levels allowing shorter integration times and operation at frame rates exceeding 400 Hz is technically possible with increased on-chip binning and a consequential reduction in spatial resolution.

The system has recently been commissioned on MAST during a period when only one of the two NBI beam-lines was operational to allow the second beam-line to be upgraded. A new, long-pulse JET-type PINI is being installed on this beam-line which will deliver 2.5 MW at 75 kV in D^0 for up to 5s (the second beam-line is to be upgraded later). The higher D^0 injection energy compared to the 50 keV delivered by the old sources, will result in improved beam penetration to the core and an increased CX cross-section. The new beam will also be of smaller diameter resulting in increased brightness. The facility to chop or 'notch' the beam will also be provided, which will allow background emission during the period of the beam notches to be subtracted from the CXRS spectra. All of these attributes will further improve the quality of the CXRS data.

Results

Most elements of the new CXRS system have now been commissioned on MAST and calibrated. Currently, ion temperature T_i and toroidal rotation velocity v_ϕ profiles are produced routinely by a post-shot analysis code for a single time-slice at the time of the neutral beam cut-off. (The ability to notch the beam with the new PINI will facilitate determination of the T_i and v_ϕ profile evolution and the analysis software for this is under development.)

Profiles of T_i and v_ϕ are shown in Fig. 3 measured during two shots: a typical high-performance H-mode plasma (#13035, $I_p \sim 750$ kA, $B_T \sim 0.6$ T, line-average density, $\bar{n}_e \sim 3\times10^{19}$ m^{-3}) and an L-mode plasma (#12546, with similar plasma parameters). The temperature profiles are remarkably similar, the increased energy confinement of the H-mode being mainly due to a broader density profile. In the plasma periphery, T_e somewhat exceeds T_i in both discharges. This difference can strongly influence the results of thermal transport analysis as the electron-ion exchange power becomes appreciable at the low temperatures observed in this region. The extent to which the difference may arise from systematic errors in the CXRS or TS data is currently being investigated.

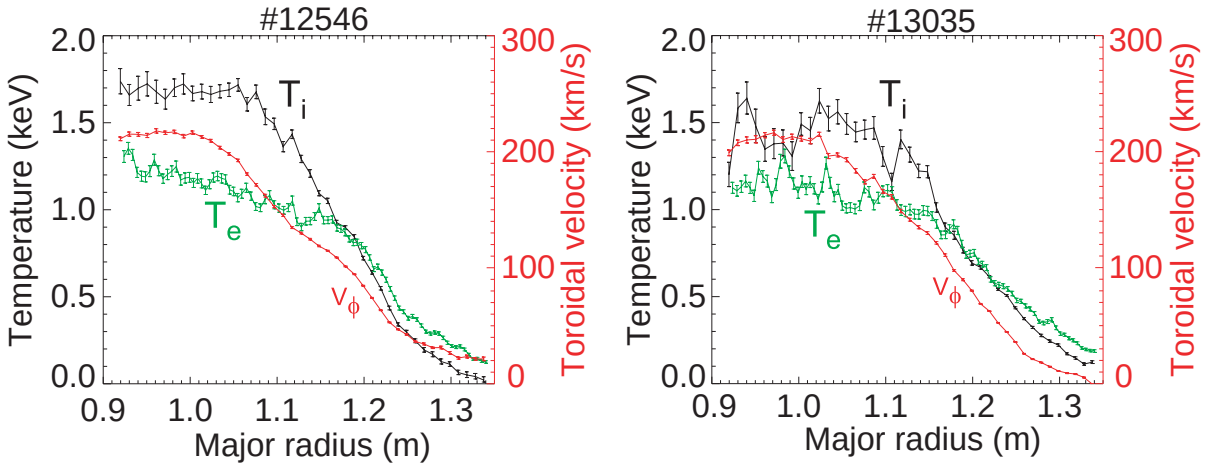

Figure 3: Temperature and rotation profiles for #12546 (L-mode) and #13035 (H-mode)

Preliminary TRANSP runs have been performed using data from the TS system for the electron channel, the new CXRS system for the C^{6+} ion temperature and toroidal rotation profiles and the high resolution 2D visible-Bremsstrahlung imaging system for the effective ion charge, Z_{eff}, profile. The evolution of the magnetic equilibrium was determined by solving the poloidal field diffusion equation, assuming neo-classical resistivity. Profiles of the ion and electron thermal diffusivities, χ_i and χ_e, are compared with calculated ion neo-classical values χ_i^{NC} from NCLASS [9] in Fig. 4. In both discharges, the lowest values of χ_i are observed in the half-radius region, where $\chi_i \sim$ 2-3 χ_i^{NC}. The gradient of v_ϕ, and hence the E×B shearing rate, is also strongest in this region, suggesting that anomalous transport may be reduced.

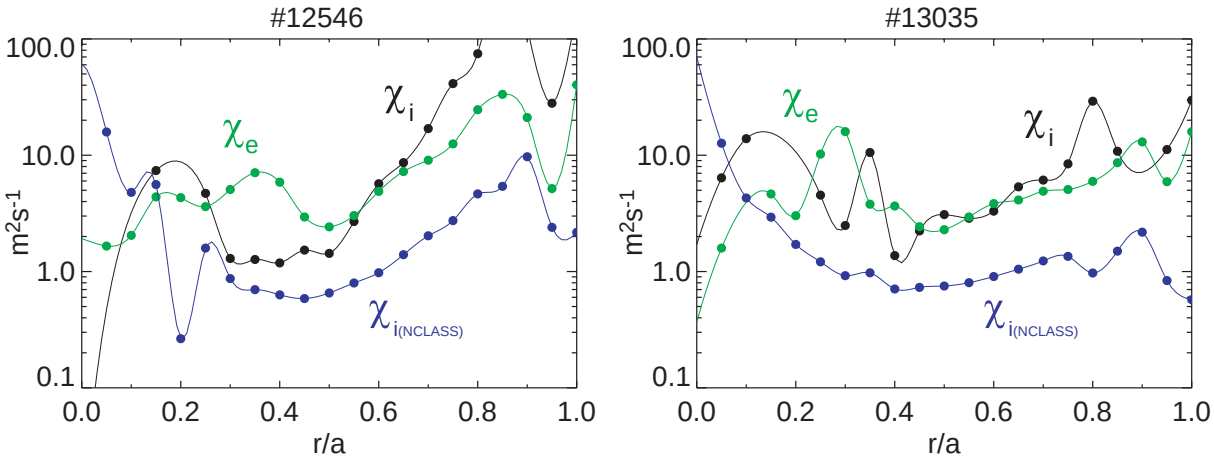

Figure 4: Thermal diffusivity profiles from TRANSP

Discussion

An upgraded CXRS diagnostic is now operational on MAST, with greatly improved spatial resolution ($\Delta R \sim 1$ cm $\sim \rho_i$), 5ms time resolution and simultaneous measurements from 224 spatial channels. With the completion of the CXRS upgrade, MAST is now better equipped to undertake detailed transport studies. Preliminary results from these studies are already available, although uncertainties on the derived transport coefficients still have to be quantified.

References

[1] A. R. Field, et al., 20th IAEA Fusion Energy Conference, 2004, Vilamoura, EX/P2-11.
[2] B. P. LeBlanc et al., Nucl. Fusion, **44** (2004) 513-523.
[3] C. M. Roach, et al., "Theory of Fusion Plasmas", Proceedings of Joint Varenna-Lausanne International Workshop, Varenna, 2004.
[4] M.R. de Baar et al., Phys. Rev. Lett. **94**, 035002 (2005)
[5] A.R. Field et al., 30th EPS, St. Petersburg, 2003, P3-93.
[6] M.J. Walsh et al., Rev. Sci. Instrum., **74,** 1663-1666 (2004)
[7] N.J. Conway et al., Rev. Sci. Instrum. **70**, 934-938 (1999).
[8] S.C. Barden et al., Proc. SPIE **4485**, 429-438 (2002)
[9] W.A. Houlberg et al., Phys. Plasmas **4** 3230 (1997)

This work was funded jointly by the United Kingdom Engineering and Physical Sciences Research Council and by the European Communities under the contract of Association between EURATOM and UKAEA. The views and opinions expressed herein do not necessarily reflect those of the European Commission.